Supporting Information

for

Transport-Relevant Pore Limiting Diameter for Molecular Separations in Metal-Organic Framework Membranes

Ting-Hsiang Hung[1], Qiang Lyu[2,3], Li-Chiang Lin[1,3,*], and Dun-Yen Kang[1,*]

[1]*Department of Chemical Engineering, National Taiwan University, No. 1, Sec. 4, Roosevelt Road, Taipei 10617, Taiwan*

[2]*School of Materials Science and Engineering, China University of Petroleum (East China), Qingdao, Shandong 266580, China*

[3]*William G. Lowrie Department of Chemical and Biomolecular Engineering, The Ohio State University, 151 W. Woodruff Avenue, Columbus, Ohio 43210, United States*

Li-Chiang Lin *E-mail: lclin@ntu.edu.tw

Dun-Yen Kang *E-mail: dunyen@ntu.edu.tw

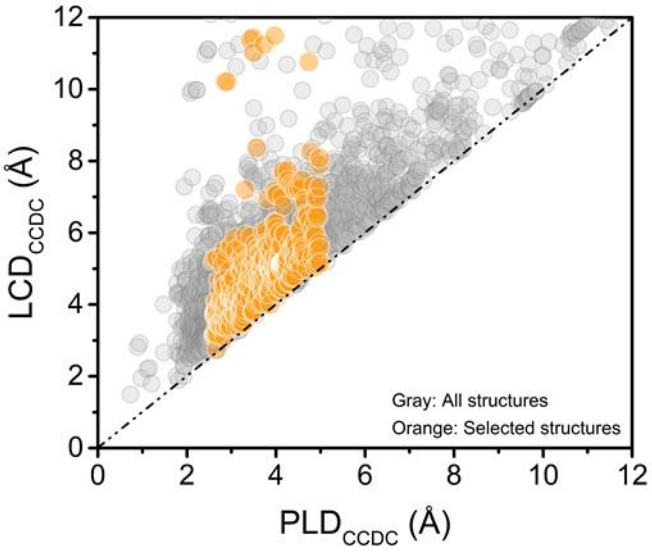

Figure S1. Topological analysis of 2932 structures included in the CoRE MOF database,[1] and 422 structures studied in this work were colored by orange.

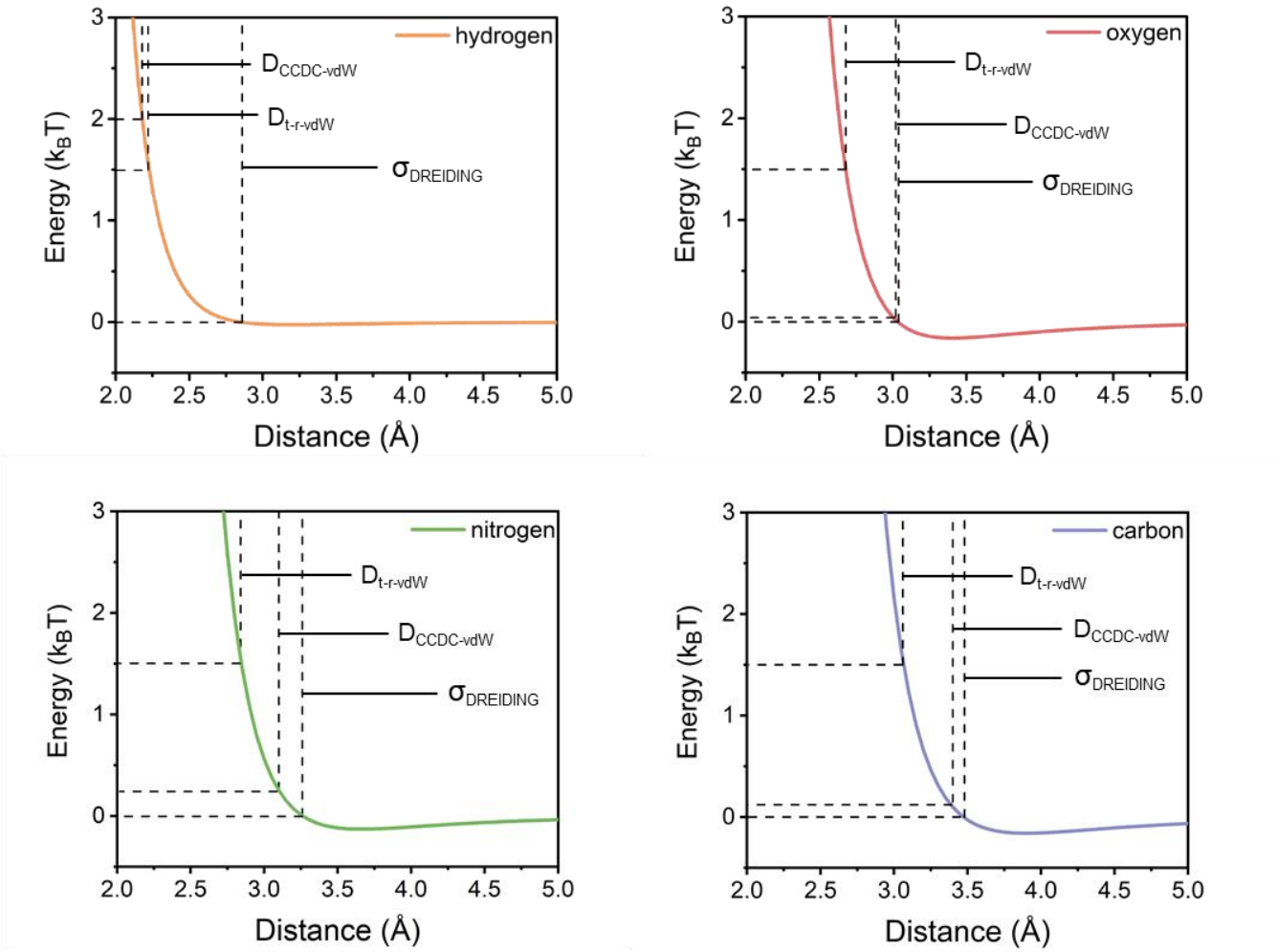

Figure S2. Lennard-Jones potential profiles of hydrogen, oxygen, nitrogen, and carbon atoms described per the DREIDING force field. The interaction energy (*y*-axis) is presented in terms of k_BT with T = 300 K. Specific distances were labeled to indicate the corresponding van der Waals diameters per different definitions.

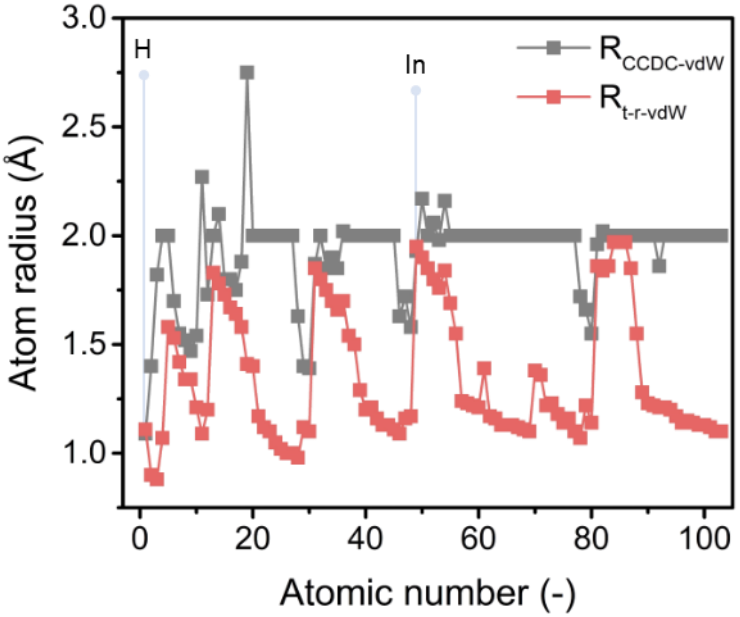

Figure S3. Atomic radius as a funtion of atomic number.

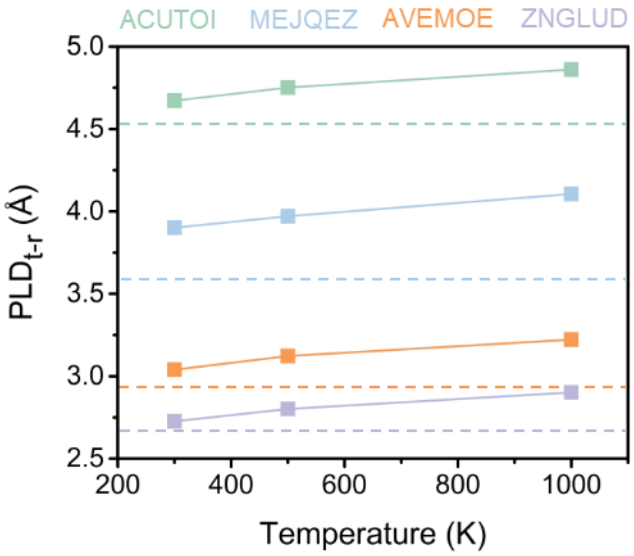

Figure S4. $PLD_{t\text{-}r}$ as a function of temperature for the four representative structures (ACUTOI, MEJQEZ, AVEMOE, and ZNGLUD in descending order of their PLD value). The horizontal dashed lines indicate the PLD_{CCDC} for each of the four structures.

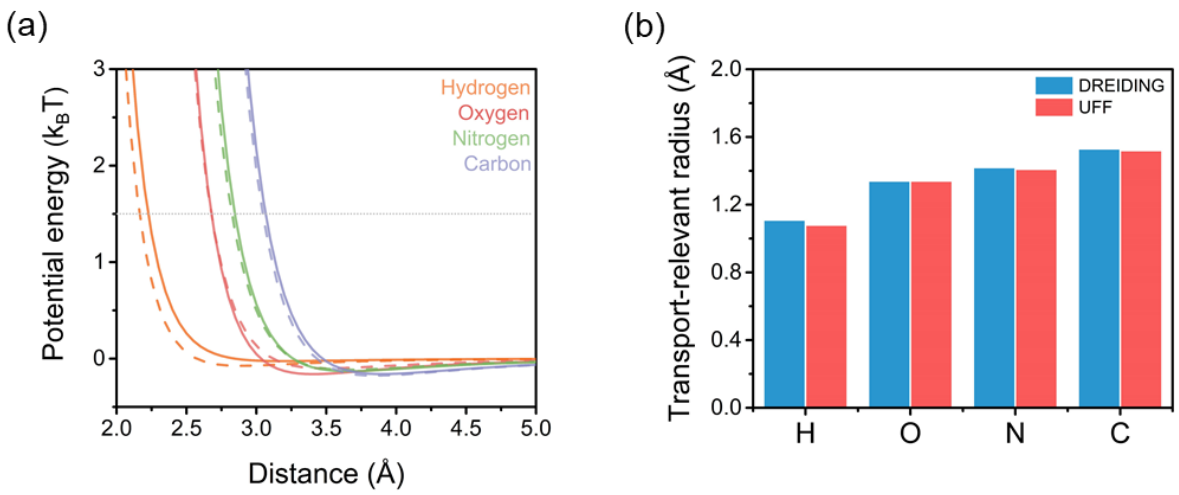

Figure S5. (a) The Lennard-Jones potential energy profiles of hydrogen, oxygen, nitrogen, and carbon atoms described per the DREIDING (solid line) and UFF (dashed line) force field. The interaction energy (*y*-axis) is presented in terms of k_BT with T = 300 K. (b) Transport-relevant radius of 4 representative elements derived from the DREIDING and UFF force fields at 300 K.

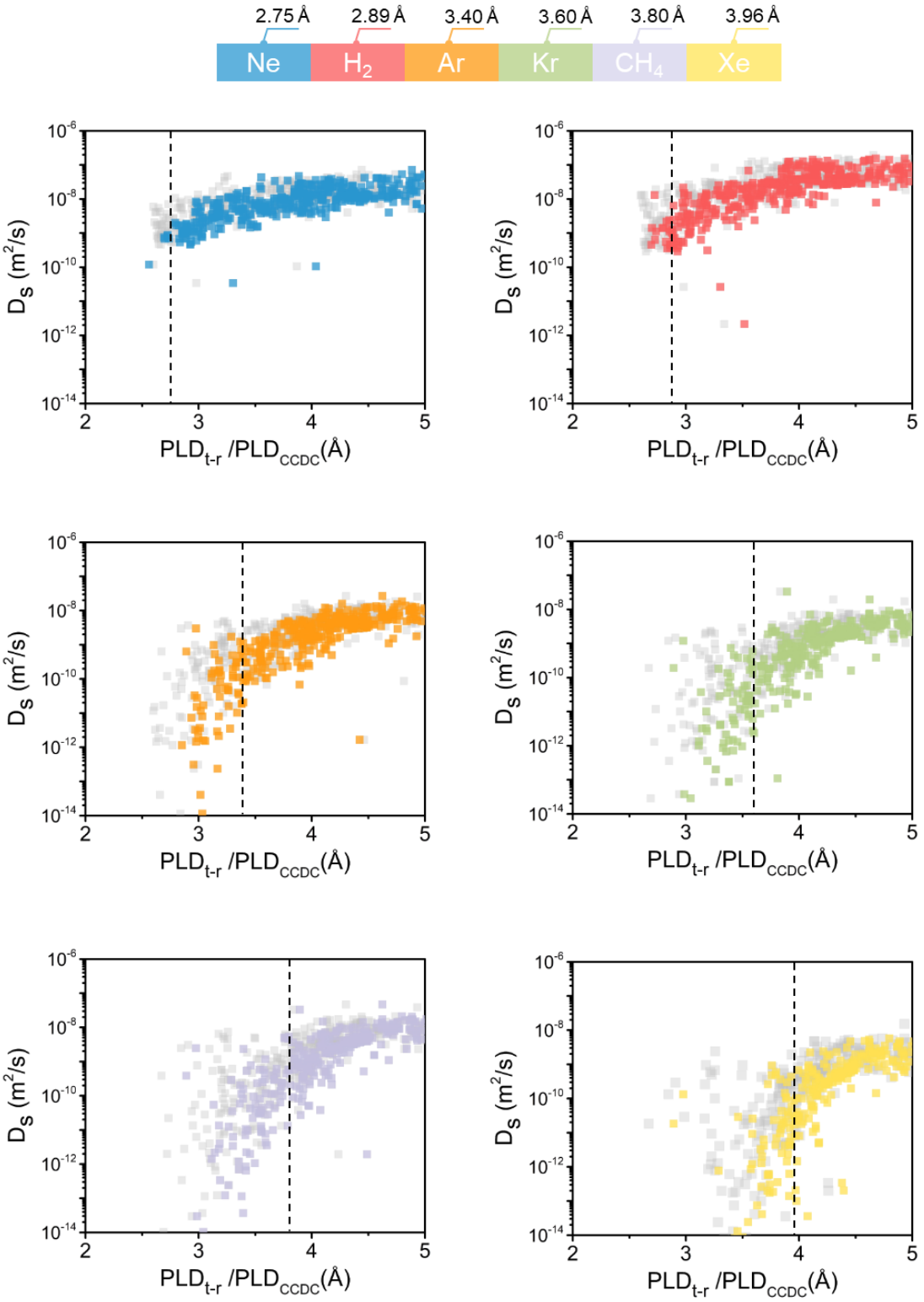

Figure S6. Self-diffusivity as a function of PLD_{CCDC} (gray) as well as $PLD_{t\text{-}r}$ (colored) at 300 K. The vertical dashed line indicates the kinetic diameter of the corresponding gas molecule.

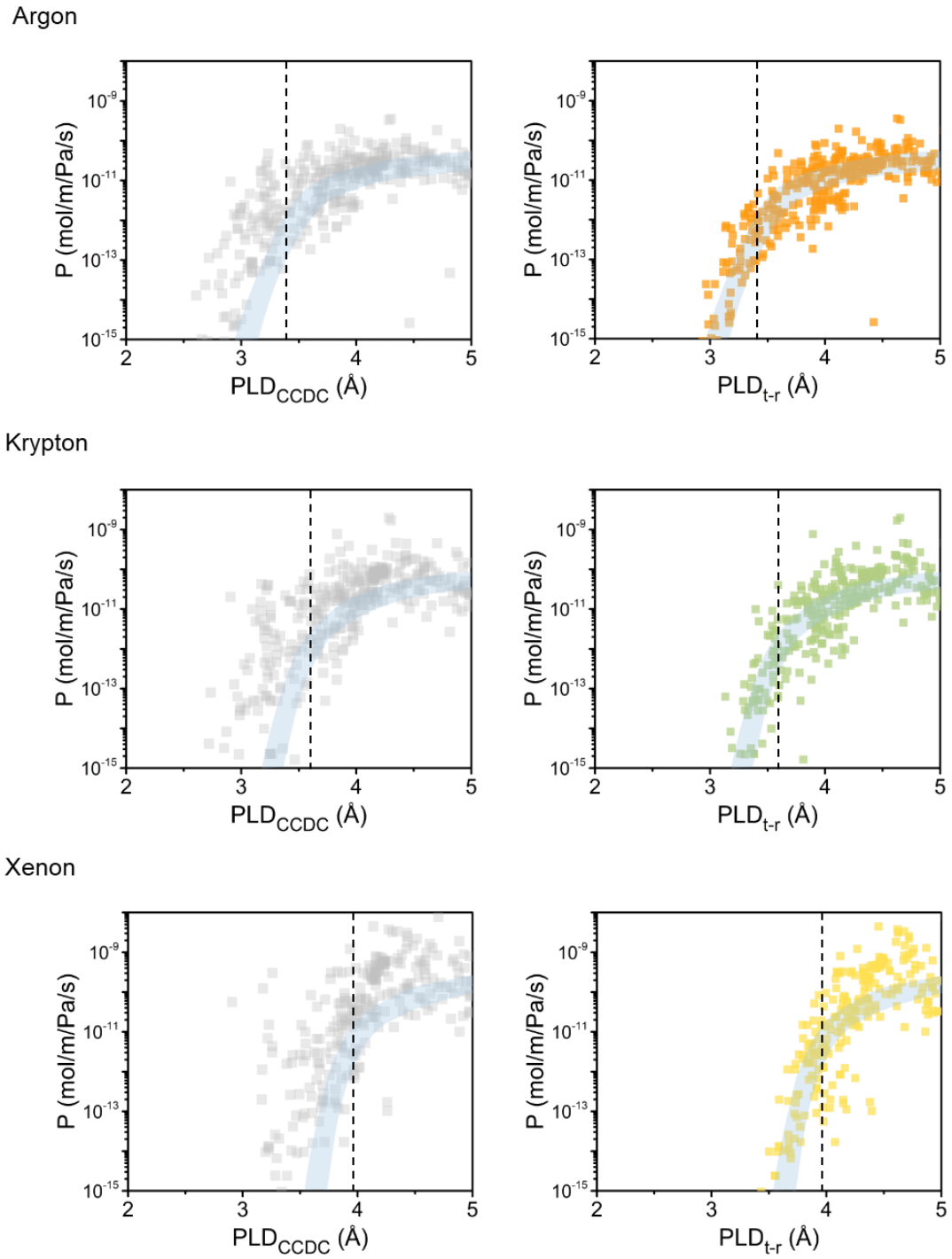

Figure S7. Permeability as a function of PLD_{CCDC} as well as PLD_{t-r} at 300 K. The blue region serves as a visual guide to the convergence of the data points, and its dimension is identical in every figure. The vertical dashed line in each figure represents the KD of the gas molecule.

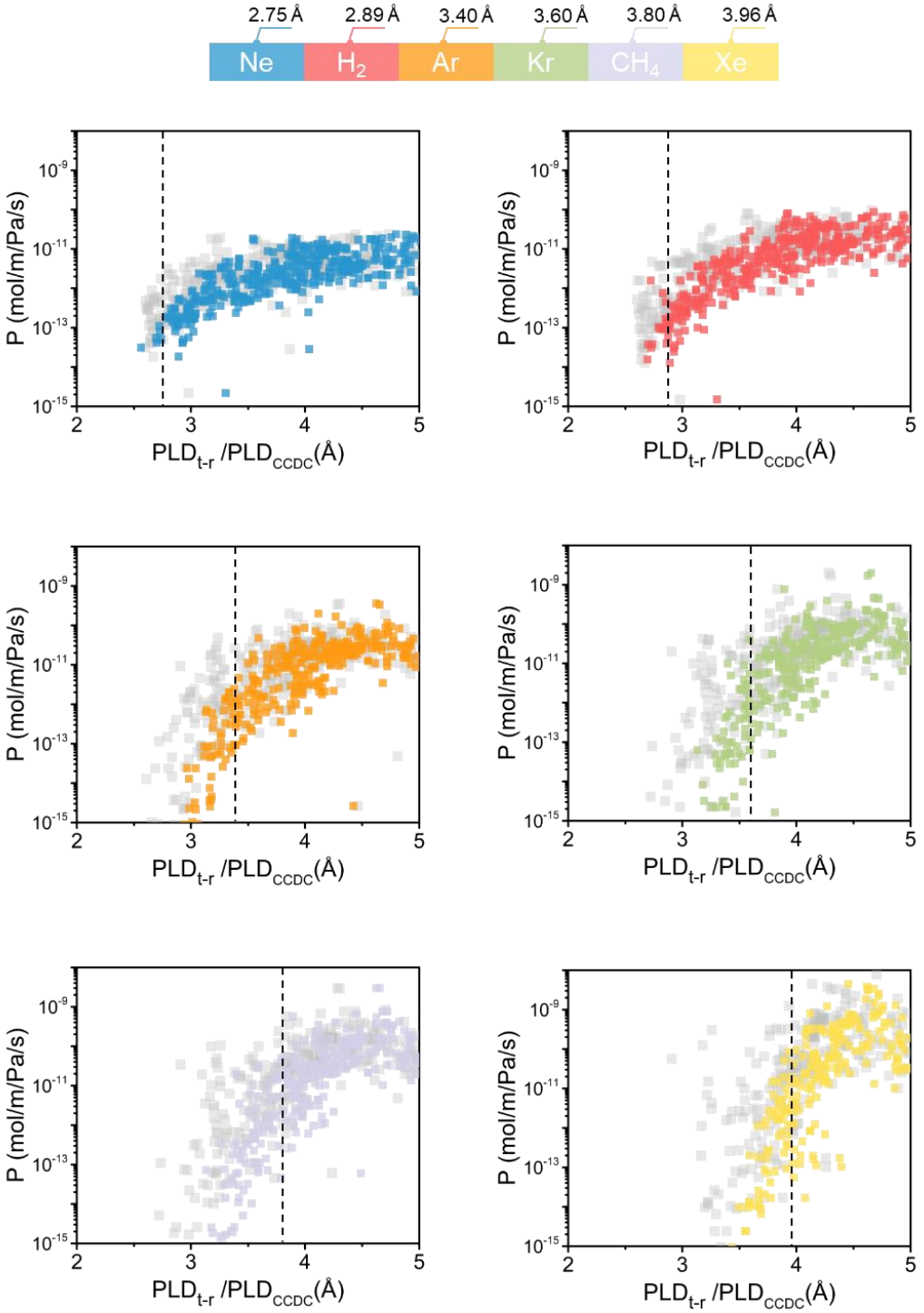

Figure S8. Permeability as a function of PLD_{CCDC} (gray) as well as $PLD_{t\text{-}r}$ (colored) at 300 K. The vertical dashed line indicates the kinetic diameter of the corresponding gas molecule.

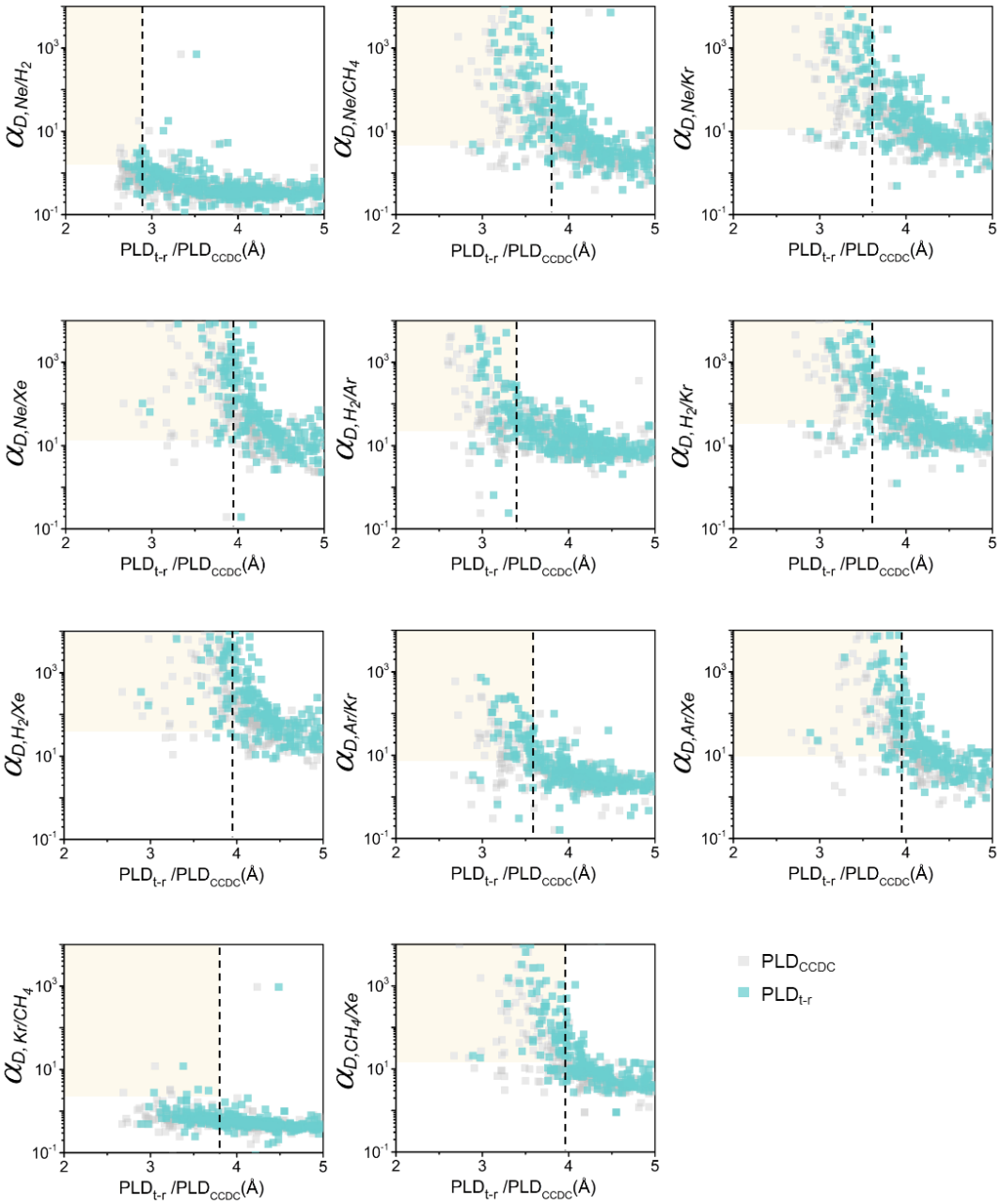

Figure S9. Diffusive selectivity as a function of PLD at 300 K. The vertical line indicates the kinetic diameter of the larger gas molecule in a binary gas mixture. Highlighted region in yellow demonstrates area where the diffusive selectivity, α_D, is higher than five times of the Knudsen selectivity and the PLD value is smaller than the kinetic diameter of the larger species in the binary mixture.

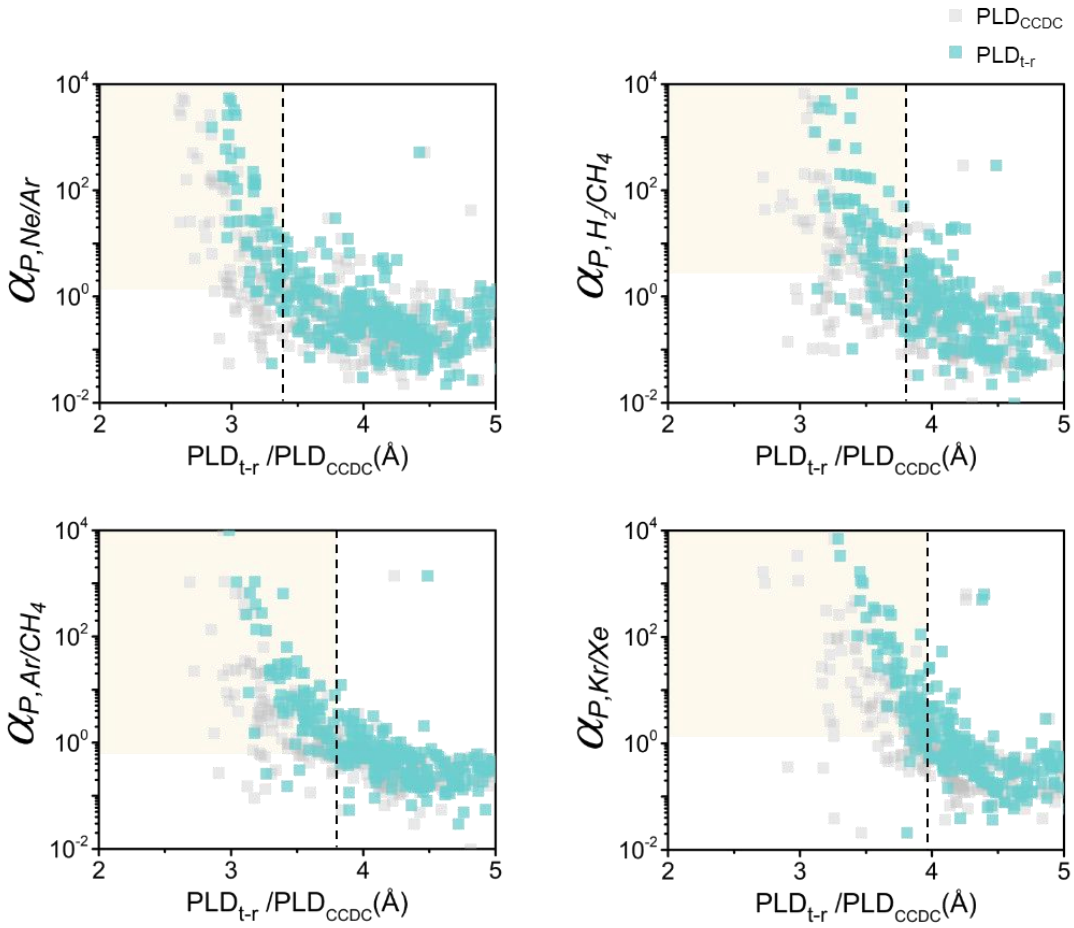

Figure S10. Permeative selectivity as a function of PLD at 300 K. The vertical line indicates the kinetic diameter of the larger gas molecule in a binary gas mixture. Highlighted region in yellow demonstrates area where the permeative selectivity, α_P, is higher than the Knudsen selectivity and the PLD value is smaller than the kinetic diameter of the larger species in the binary mixture. (The same gas mixtures as those shown in Figure 4 of the main text)

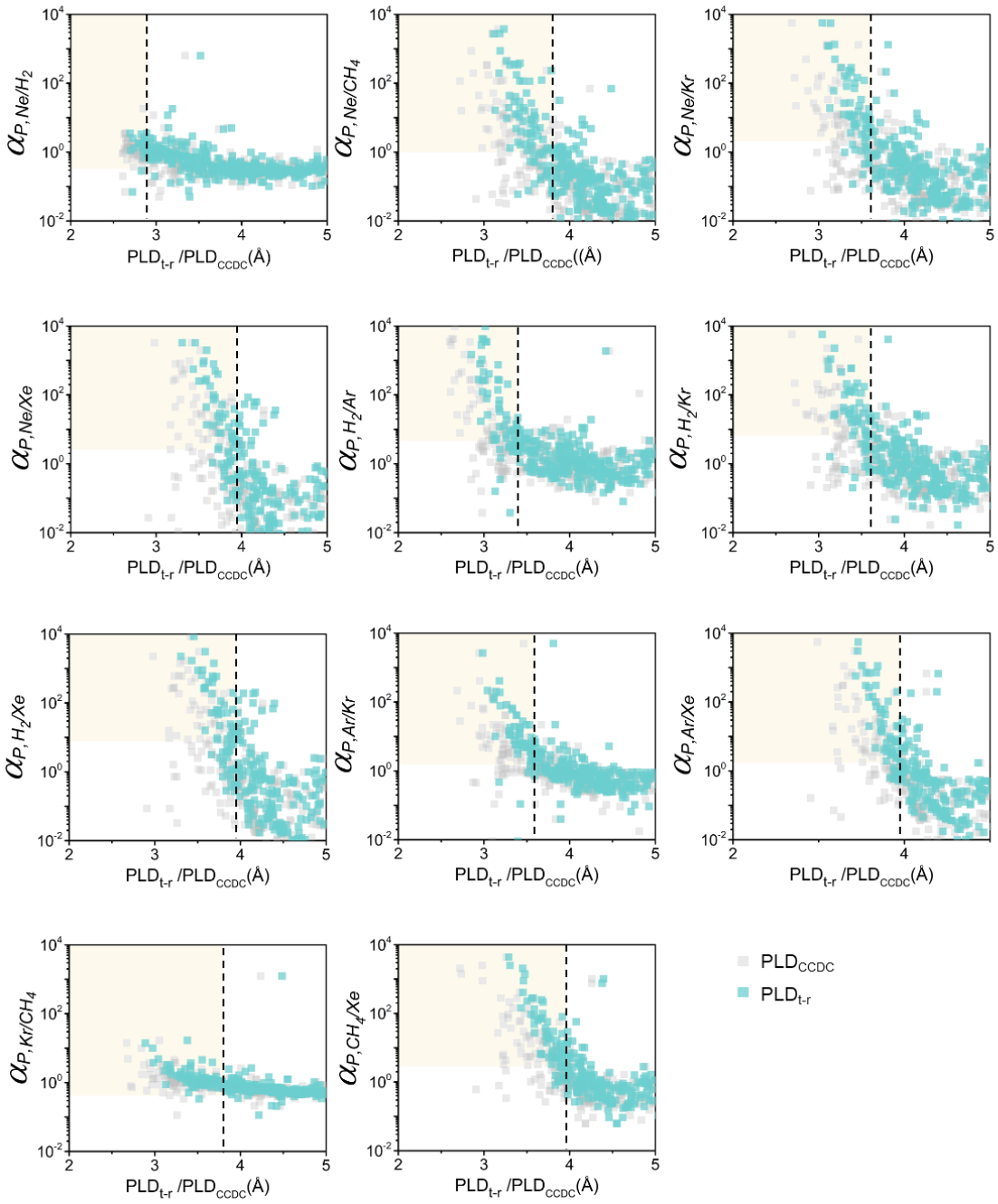

Figure S11. Permeative selectivity as a function of PLD at 300 K. The vertical line indicates the kinetic diameter of the larger gas molecule in a binary gas mixture. Highlighted region in yellow demonstrates area where the permeative selectivity, α_P, is higher than the Knudsen selectivity and the PLD value is smaller than the kinetic diameter of the larger species in the binary mixture.

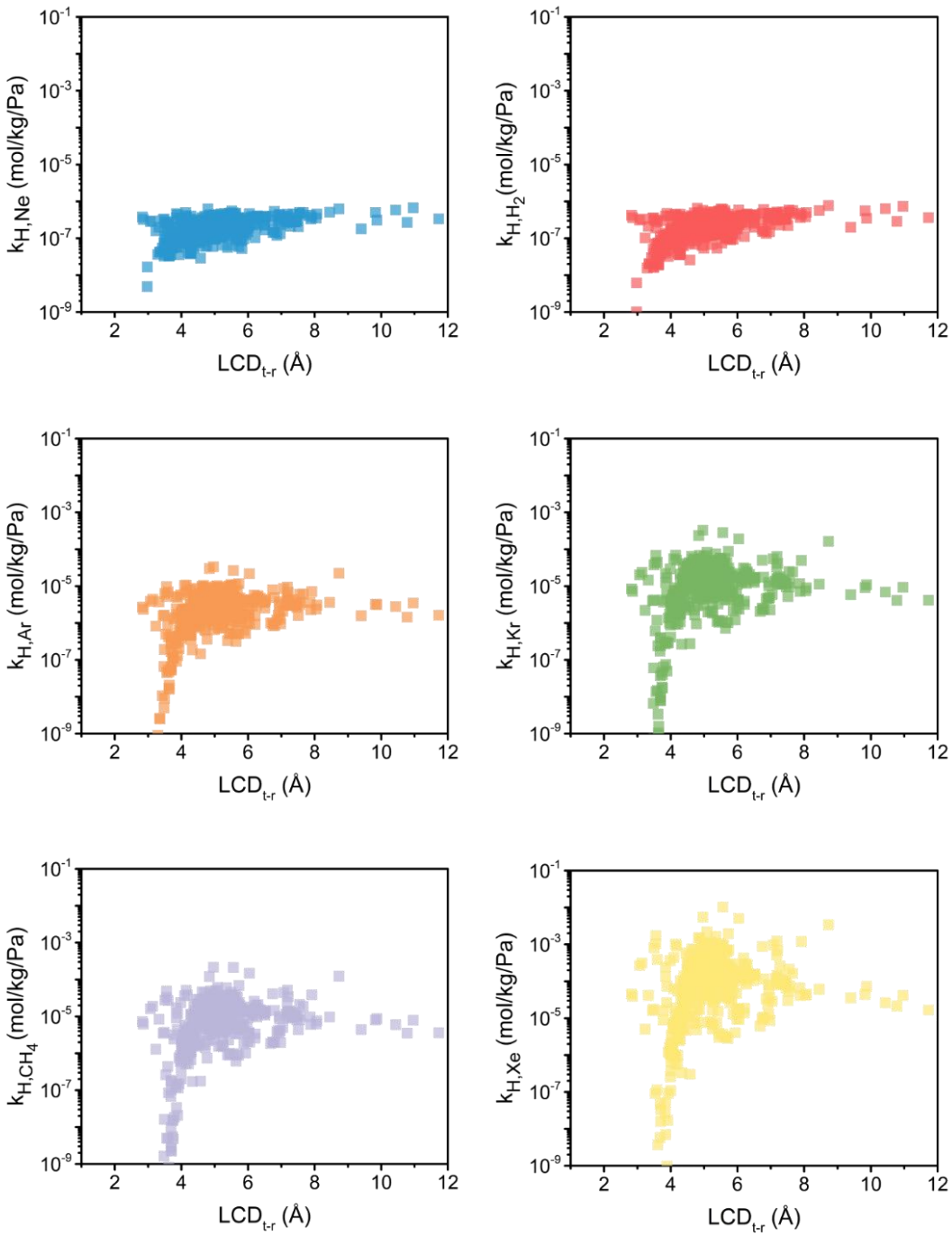

Figure S12. Henry's constant as a function of largest cavity diameter (LCD) computed based on the set of transport-relevant van der Waals radii at 300 K.

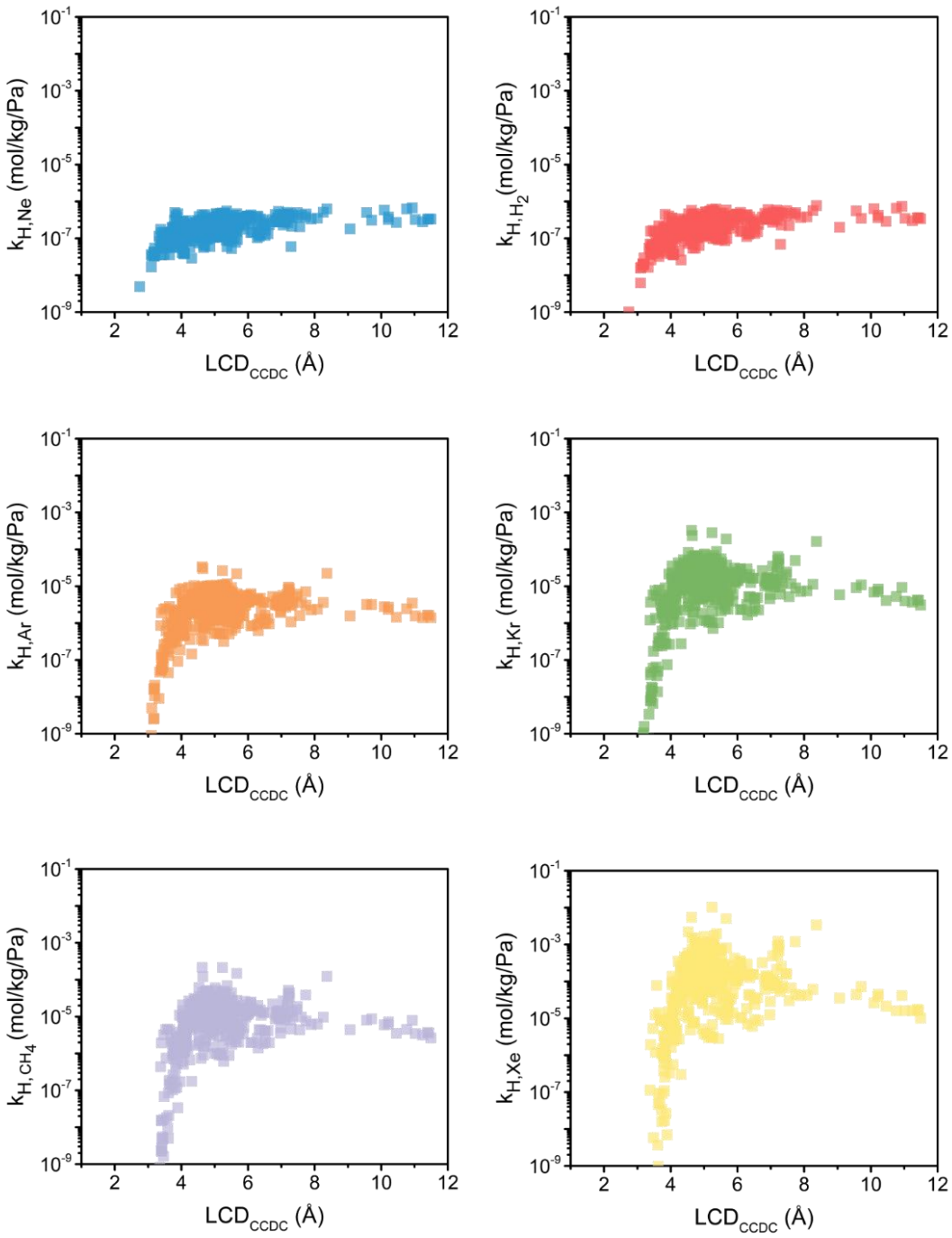

Figure S13. Henry's constant as a function of largest cavity diameter (LCD) computed based on the set of van der Waals radii outlined by CCDC at 300 K.

Table S1. Van der Waals radii for different elements. These values can be implemented in any available packages for geometric analysis. For instance, in Zeo++, one will need to modify the default radii values in a function called "initializeRadTable" in networkinfo.cc)

Element	$R_{CCDC\text{-}vdW}$	$R_{t\text{-}r\text{-}vdW}$ (300 K)
H	1.09	1.11
He	1.4	0.9
Li	1.82	0.88
Be	2	1.07
B	2	1.58
C	1.7	1.53
N	1.55	1.42
O	1.52	1.34
F	1.47	1.34
Ne	1.54	1.21
Na	2.27	1.09
Mg	1.73	1.2
Al	2	1.83
Si	2.1	1.78
P	1.8	1.73
S	1.8	1.67
Cl	1.75	1.64
Ar	1.88	1.58
K	2.75	1.41
Ca	2	1.4
Sc	2	1.17
Ti	2	1.12
V	2	1.1
Cr	2	1.05
Mn	2	1.02
Fe	2	1
Co	2	1
Ni	1.63	0.98
Cu	1.4	1.12
Zn	1.39	1.1
Ga	1.87	1.85
Ge	2	1.8

Table S1. *(Continued)*

Element	$R_{CCDC\text{-}vdW}$	$R_{t\text{-}r\text{-}vdW}$ (300 K)
As	1.85	1.75
Se	1.9	1.7
Br	1.85	1.66
Kr	2.02	1.7
Rb	2	1.54
Sr	2	1.5
Y	2	1.29
Zr	2	1.2
Nb	2	1.21
Mo	2	1.16
Tc	2	1.13
Ru	2	1.13
Rh	2	1.11
Pd	1.63	1.09
Ag	1.72	1.16
Cd	1.58	1.17
In	1.93	1.95
Sn	2.17	1.9
Sb	2	1.85
Te	2.06	1.8
I	1.98	1.76
Xe	2.16	1.84
Cs	2	1.69
Ba	2	1.55
La	2	1.24
Ce	2	1.23
Pr	2	1.22
Nd	2	1.21
Pm	2	1.39
Sm	2	1.17
Eu	2	1.16
Gd	2	1.13
Tb	2	1.13
Dy	2	1.13
Ho	2	1.12
Er	2	1.11
Tm	2	1.1

Table S1. *(Continued)*

Element	$R_{CCDC\text{-}vdW}$	$R_{t\text{-}r\text{-}vdW}$ (300 K)
Yb	2	1.38
Lu	2	1.36
Hf	2	1.22
Ta	2	1.23
W	2	1.18
Re	2	1.14
Os	2	1.16
Ir	2	1.1
Pt	1.72	1.07
Au	1.66	1.22
Hg	1.55	1.14
Tl	1.96	1.86
Pb	2.02	1.84
Bi	2	1.86
Po	2	1.97
At	2	1.97
Rn	2	1.97
Fr	2	1.85
Ra	2	1.55
Ac	2	1.28
Th	2	1.23
Pa	2	1.22
U	1.86	1.21
Np	2	1.21
Pu	2	1.2
Am	2	1.17
Cm	2	1.14
Bk	2	1.15
Cf	2	1.14
Es	2	1.13
Fm	2	1.13
Md	2	1.12
No	2	1.1
Lw	2	1.1
Rf	2	N/A

Table S1. *(Continued)*

Element	$R_{CCDC\text{-}vdW}$	$R_{t\text{-}r\text{-}vdW}$ (300 K)
Db	2	N/A
Sg	2	N/A
Bh	2	N/A
Hs	2	N/A
Mt	2	N/A
Ds	2	N/A

Table S2. Van der Waals repulsive force between two proximate atoms at the distance of $D_{CCDC\text{-}vdW}$ and $D_{t\text{-}r\text{-}vdW}$ for four representative elements. The repulsive force computed at the distance of our proposed $D_{t\text{-}r\text{-}vdW}$ are consistent for four of these elements (i.e., 2728 ± 201 K/Å), whereas the repulsion is largely varied from as small as 365 to as large as 3716 at a distance of $D_{CCDC\text{-}vdW}$.

Element	Repulsive force [K/Å]	
	$D_{CCDC\text{-}vdW}$	$D_{t\text{-}r\text{-}vdW}$
H	3716	2783
C	488	2554
N	704	2646
O	365	2929

Table S3. Lennard-Jones parameters of DREIDING and UFF force field and the corresponding transport-relevant radii at 300 K.

	DREIDING			UFF		
	ε [K]	σ [Å]	$R_{t\text{-}r\text{-}vdW}$ [Å]	ε [K]	σ [Å]	$R_{t\text{-}r\text{-}vdW}$ [Å]
H	7.65	2.85	1.11	22.13	2.57	1.09
O	48.14	3.03	1.34	30.18	3.12	1.34
N	38.93	3.26	1.42	34.71	3.26	1.41
C	47.84	3.47	1.53	52.81	3.43	1.52

Table S4. Spearman's rank correlation coefficient (ρ) between the logarithm of diffusive selectivity and the PLD value calculated with different sets of van der Waals radii. The results shown in this table only considered those structures with an aperture size of less than 4 Å.

	ρ of PLD_{CCDC} and log (α_D)	ρ of $PLD_{t\text{-}r}$ and log (α_D)	Improvement (%)
Ne/H_2	-0.628	-0.660	3.2
Ne/Ar	-0.637	-0.663	2.5
Ne/Kr	-0.549	-0.620	7.1
Ne/CH_4	-0.512	-0.598	8.6
Ne/Xe	-0.450	-0.580	12.9
H_2/Ar	-0.515	-0.577	6.2
H_2/Kr	-0.420	-0.546	12.6
H_2/CH_4	-0.424	-0.552	12.8
H_2/Xe	-0.325	-0.517	19.2
Ar/Kr	-0.483	-0.614	13.1
Ar/CH_4	-0.446	-0.578	13.2
Ar/Xe	-0.346	-0.553	20.8
Kr/CH_4	-0.391	-0.503	11.2
Kr/Xe	-0.396	-0.595	19.8
CH_4/Xe	-0.426	-0.607	18.1

Table S5. Spearman's rank correlation coefficient (ρ) between the logarithm of permeative selectivity and the PLD value calculated with different sets of van der Waals radii. The results shown in this table only considered those structures with an aperture size of less than 4 Å.

	ρ of PLD_{CCDC} and log (α_P)	ρ of $PLD_{t\text{-}r}$ and log (α_P)	Improvement (%)
Ne/H_2	-0.522	-0.552	3.0
Ne/Ar	-0.673	-0.699	2.5
Ne/Kr	-0.592	-0.635	4.3
Ne/CH_4	-0.591	-0.651	6.0
Ne/Xe	-0.582	-0.659	7.7
H_2/Ar	-0.679	-0.628	-5.1
H_2/Kr	-0.662	-0.654	-0.8
H_2/CH_4	-0.680	-0.678	-0.1
H_2/Xe	-0.634	-0.672	3.8
Ar/Kr	-0.598	-0.702	10.4
Ar/CH_4	-0.621	-0.725	10.4
Ar/Xe	-0.590	-0.744	15.4
Kr/CH_4	-0.619	-0.722	10.2
Kr/Xe	-0.612	-0.766	15.5
CH_4/Xe	-0.522	-0.552	3.0

References

1. Chung, Y. G.; Camp, J.; Haranczyk, M.; Sikora, B. J.; Bury, W.; Krungleviciute, V.; Yildirim, T.; Farha, O. K.; Sholl, D. S.; Snurr, R. Q., Computation-Ready, Experimental Metal–Organic Frameworks: A Tool To Enable High-Throughput Screening of Nanoporous Crystals. *Chem. Mater.* **2014,** *26* (21), 6185-6192.